J. Fluid Mech. (2021), *vol*. 911, A58, doi:10.1017/jfm.2020.1105

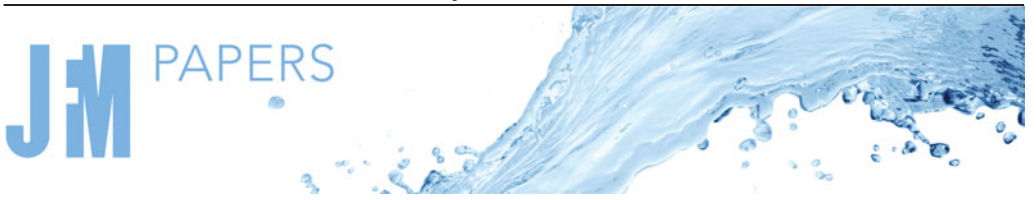

The first open channel for yield-stress fluids in porous media

Dimitrios Fraggedakis[1],†, **Emad Chaparian**[2] **and Outi Tammisola**[3]

[1]Department of Chemical Engineering, Massachusetts Institute of Technology, Cambridge, MA 02139, USA

[2]Mathematics Department, University of British Columbia, Vancouver, BC V6T 1Z2, Canada

[3]Linné FLOW centre, Department of Engineering Mechanics, KTH Royal Institute of Technology, SE-10044 Stockholm, Sweden

(Received 15 August 2020; revised 31 October 2020; accepted 1 December 2020)

The prediction of the first fluidized path of yield-stress fluids in complex porous media is a challenging yet important task to understand the fundamentals of fluid flow in several industrial and biological processes. In most cases, the conditions that open this first path are known either through experiments or expensive computations. Here, we present a simple network model to predict the first open channel for a yield-stress fluid in a porous medium. For porous media made of non-overlapping discs, we find that the pressure drop ΔP_c required to open the first channel for a given yield stress τ_y depends on both the relative discs size R_s to the macroscopic length L of the system and the packing fraction ϕ. The non-dimensional pressure gradient $\Delta P_c R_s/\tau_y L$ (i.e. the critical yield number), however, depends on the packing fraction ϕ only, leading to a mastercurve for all examined ratios of R_s/L. In the case of non-overlapping discs, we find $\Delta P_c R_s/\tau_y L \sim \phi/(1-\phi)$. We also report the statistics on the arclength of the first open path. Finally, we discuss the implication of our results for the design of porous media used in energy storage applications.

Key words: porous media, plastic materials

1. Introduction

Fluid flows in porous media have been studied for more than a century due to their high relevance to several engineering applications such as enhanced oil recovery (Green & Willhite 1998; Sahimi 2011; Farajzadeh *et al.* 2012; Fraggedakis *et al.* 2015), filtration and separation (Herzig, Leclerc & Goff 1970; Tien & Payatakes 1979; Jaisi *et al.* 2008), fermentation (Pandey 2003; Aufrecht *et al.* 2019), soil sequestration (Schlesinger

† Email address for correspondence: dimfraged@gmail.com

1999), energy storage (Duduta *et al.* 2011; Sun *et al.* 2019) and food processing (Greenkorn 1983). In most cases, the fluids involved in these applications exhibit yield stress/viscoplastic behaviour (Bonn & Denn 2009; Balmforth, Frigaard & Ovarlez 2014). Thus, understanding the conditions – critical pressure drop and/or stresses – that lead to fluidization of yield-stress fluids in porous media can help boost the efficiency and lower the operational cost of several industrial applications.

In pressure-driven flows, the critical pressure drop ΔP_c required to fluidize the yield-stress fluid and open the first channel (Chen, Rossen & Yortsos 2005; Hewitt *et al.* 2016; Waisbord *et al.* 2019) depends on the heterogeneous geometric characteristics and porosity $1-\phi$ of the porous medium, where ϕ is the volume fraction of the solid phase (Talon *et al.* 2013; Bauer *et al.* 2019; Chaparian & Tammisola 2021). Therefore, it is crucial to understand the relation between the yielding conditions and the structure of the porous medium, which will lead to predictive models for both the first open channel and ΔP_c. The classic studies in this era date back to the 1950s and 1960s; the main concern was filtration and oil recovery and limiting pressure gradient models have been proposed (e.g. see Entov 1967; Barenblatt, Entov & Ryzhik 1989). A brief review on the history of the field can be found in Frigaard, Paso & de Souza Mendes (2017).

The classical way to study yield-stress fluids is by solving the momentum equations using viscoplastic constitutive relations, such as the Bingham and Herschel–Bulkley models (Huilgol 2015; Saramito 2016). The yield-stress behaviour, however, leads to an ill-defined problem that does not describe the stress distribution within the unyielded regions of the fluid (Balmforth *et al.* 2014; Saramito & Wachs 2017). Common ways to resolve this problem are by using either optimization- (Hestenes 1969; Powell 1978; Glowinski 2008; Glowinski & Wachs 2011) or regularization-based methods (Papanastasiou 1987; Frigaard & Nouar 2005). The former are accurate in predicting the yielded/unyielded boundaries and the flow field, however, they are computationally expensive, especially near the yield limit (Saramito & Wachs 2017). Although the latter reduce the computational cost, they introduce non-physical parameters that lead to non-physical solutions, incorrect location of yield/unyield boundaries and inaccurate yield limits (Frigaard & Nouar 2005; Tsamopoulos *et al.* 2008; Dimakopoulos, Pavlidis & Tsamopoulos 2013). Here, we are interested in determining the statistics of the critical ΔP_c for a yield-stress fluid in a porous medium. Thus, we need to use models that can predict accurately and efficiently ΔP_c along with the first open channel.

Fluid flow in a porous medium is traditionally described through network models (Fatt 1956) that represent the complex geometric characteristics of the domain with spherical pore throats and cylindrical edges (Bryant, King & Mellor 1993; Blunt 2001; Blunt *et al.* 2013; Alim *et al.* 2017; Stoop *et al.* 2019). In addition to their wide applicability in Newtonian fluids, network models have also been applied to describe ΔP_c and the flow behaviour with respect to the applied pressure drop in yield-stress fluids (Balhoff & Thompson 2004; Balhoff 2005; Chen *et al.* 2005; Sochi 2005; Balhoff *et al.* 2012; Liu *et al.* 2019; Talon & Hansen 2020). When the relation between the local flow rate and the pressure drop is known, the network representation allows for the use of graph theoretic tools (Kharabaf & Yortsos 1997; Chen *et al.* 2005; Balhoff *et al.* 2012; Liu *et al.* 2019) to quickly evaluate ΔP_c and the flow response of the system. In general, however, the results of network viscoplastic models in complex porous media have been rarely compared and validated against those produced by solving the full fluid problem, and thus the conditions of their validity/applicability are still unknown.

The goal of the present work is to predict the first open channel for a yield-stress fluid in a porous medium along with the critical applied pressure drop required to open it.

We develop a simple network model based on realistic porous medium configurations, and use graph theoretical tools to study the statistics of the yielding conditions in terms of the medium porosity. We validate our results against pressure-driven simulations of Bingham fluids in porous media. Indeed, we bridge the gap between the continuum flow approaches and network models and also report/analyse the functionality of the critical pressure drop on the porosity. Finally, we discuss the relevance of our study to applications such as semi-solid flow batteries and propose possible extensions.

2. Theory

2.1. *Network generation and topology*

We are interested in the construction of realistic network models that capture the complex morphology of real porous media. The main scope of our work is to understand the statistics of the critical conditions that lead to fluidization in terms of the porosity $1 - \phi$ and the topological characteristics of the medium.

To a first approximation, we assume a porous medium that consists of monodisperse non-overlapping discs (two-dimensional problem) of radius R_s, as shown in figure 1(*a*). It is apparent that the structure of the void space depends on the solid volume fraction defined as $\phi = N_s A_s / A_t$, where N_s is the total number of discs, $A_s = \pi R_s^2$ is the area of an individual disc and $A_t = L \times L$ the total area of the system.

For the generation of porous media that consist of non-overlapping discs, we implemented the random sequential addition algorithm (Cule & Torquato 1999; Torquato, Uche & Stillinger 2006; Zhang & Torquato 2013). The procedure described by Torquato *et al.* (2006) allows for a fast generation of randomly packed discs with the desired volume fractions. Due to the constraint of non-overlapping discs, all generated microstructures never exceed $\phi = 0.52$ in two dimensions.

Based on the generated porous medium structure, we can create its network representation as shown in the right image of figure 1(*a*). The network consists of nodes and edges that span the entire medium, where its complex topological characteristics are encoded on the connectivity between them (Gostick 2017). The local geometric characteristics of the porous medium are included in the length ℓ_i and gap $2h_i$ of each individual edge, as we show in figure 1(*b*).

For the generation of the network model, we implemented the maximal ball algorithm (Silin & Patzek 2006; Al-Kharusi & Blunt 2007; Dong & Blunt 2009) which allows us to obtain the h_i and length ℓ_i for each edge. The maximal ball algorithm 'fits' a circle/sphere within each pore (Alim *et al.* 2017), the radius of which represents h_i. As will be discussed in § 3.2, there are recently developed methods (Gostick 2017) that can extract h_i and ℓ_i using image processing, such as the watershed segmentation. Other choices of h_i can be considered (e.g. equivalent gap/radius etc.), however, our choice for the local radius works well in predicting both the first open channel and the critical pressure drop required to open it. The generated network was represented by a graph with vertices V and edges E using the open source library NetworkX (Hagberg, Swart & Chult 2008). For demonstration, we show in figure 1(*c*) the pore-size distribution for the configuration of figure 1(*a*).

2.2. *Yield-stress fluid in a network*

Yield-stress fluids are characterized by their solid–liquid transition when the Euclidean norm of the stress field exceeds the value of yield stress (i.e. von Mises criterion; see Hill 1998; Gurtin, Fried & Anand 2010). The typical shear stress response in simple shear flow

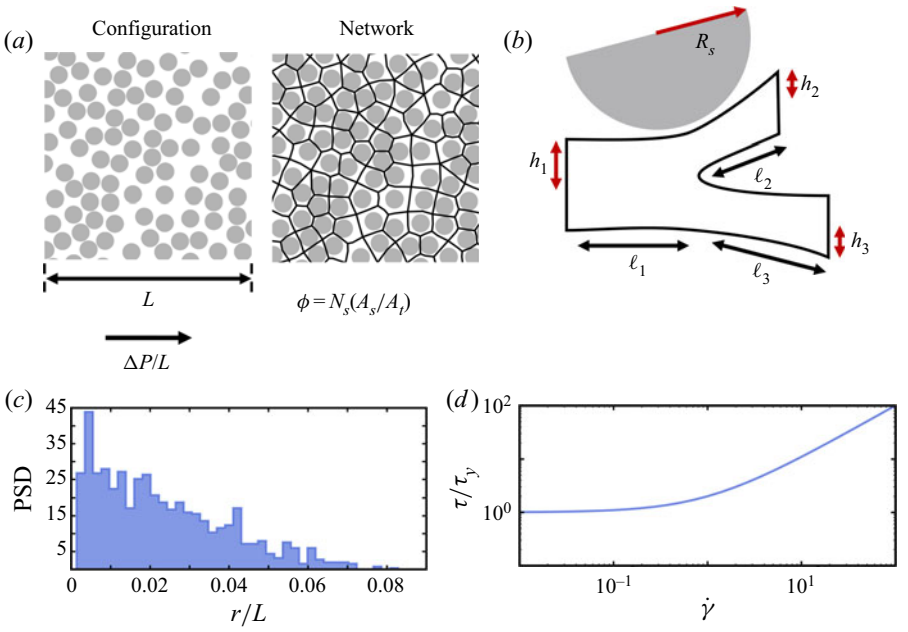

Figure 1. (*a*) Typical configuration of a porous medium of length L and porosity $1-\phi$ that is made of non-overlapping monodisperse discs of radius R_s, and its network representation. Across the domain, a macroscopic pressure gradient $\Delta P/L$ is applied. (*b*) Schematic of three network edges with different h_i and $\ell_i (i = 1, 2, 3)$. The network representation includes the local geometric characteristics of the complex porous medium structure. (*c*) Characteristic pore-size distribution for the network shown in (*a*) as derived from the network model. (*d*) Typical shear stress response τ as a function of the applied shear rate $\dot{\gamma}$ of a viscoplastic fluid with yield stress τ_y.

is shown in figure 1(*d*), where for $\dot{\gamma} \to 0$ the shear stress reaches its critical value $\tau \to \tau_y$. The most common constitutive relations used to describe 'simple' yield-stress fluids are the Bingham and Herschel–Bulkley models, which differ in their viscosity functional. Both of them, however, predict the same yield limit (Frigaard 2019) since the viscous dissipation is negligible compared to the plastic one for $\dot{\gamma} \to 0$. Therefore, it is sufficient to discuss only the Bingham model for a porous medium to understand the connection between the yielding conditions and the geometric and topological characteristics of the network.

For a Bingham fluid pressure-driven flow close to the yield limit (i.e. the linearization of the flow rule), the local flow rate q_i of edge i is described in terms of the local geometric properties h_i, ℓ_i, the local pressure drop along the edge ΔP_i and the yield stress τ_y of the fluid as,

$$q_i \sim \begin{cases} \dfrac{h_i^3}{\ell_i}\left(\Delta P_i - \dfrac{\tau_y \ell_i}{h_i}\right) & \text{for } \Delta P_i > \dfrac{\tau_y \ell_i}{h_i}, \\ 0 & \text{for } |\Delta P_i| < \dfrac{\tau_y \ell_i}{h_i}, \\ \dfrac{h_i^3}{\ell_i}\left(\Delta P_i + \dfrac{\tau_y \ell_i}{h_i}\right) & \text{for } \Delta P_i < -\dfrac{\tau_y \ell_i}{h_i}. \end{cases} \tag{2.1}$$

Near the no-flow limit $q_i \to 0$, we see from (2.1) that $\Delta P_i \to \tau_y \ell_i / h_i$, and thus channels that are smaller in radius and/or longer in length require a larger applied pressure drop to yield. This is the common yield criterion for plane Poiseuille flow of a Bingham fluid in a channel of width $2h_i$ and length ℓ_i. Across the first open channel, we can calculate the total pressure drop across the medium to be $\Delta P_c \equiv \sum_{i=1}^{N} \Delta P_{c,i} = \tau_y \sum_{i=1}^{N} \ell_i / h_i$, where N is the total number of edges across the path. From this expression, we can see that the connectivity between the edges determines the first open channel in a real porous medium, and it corresponds to the path of 'least resistance'. Thus, the problem of finding ΔP_c can be formulated as finding the path of the minimum pressure drop as follows (Liu *et al.* 2019)

$$\frac{\Delta P_c}{\tau_y} = \min_{C \in \mathcal{C}_{in-out}} \sum_{i=1}^{N} \frac{\ell_i}{h_i}, \tag{2.2}$$

where $\mathcal{C}_{in-out}$ is the set of all paths between the corresponding boundaries. The problem of (2.2) satisfies the principle of minimum dissipation rate and is valid near equilibrium (De Groot & Mazur 1984). In particular, for isothermal pressure-driven flow of temperature T, the energy dissipation according to linear irreversible thermodynamics is $\Phi = q\Delta P$ (De Groot & Mazur 1984). Thus, for conditions near the solid–liquid transition where $q \to 0^+$, the minimum pressure drop path also minimizes Φ.

To solve equation (2.2), we transform the generated network into a graph with edges that have weights equal to ℓ_i / h_i and use the Dijkstra method (Dijkstra 1959) for directed graphs to determine the first open channel. This method is known to scale quadratically with the path length (Bollobás 2013), and therefore the computational cost increases for complex domains with a larger number of edges. For a single porous medium configuration, however, the overall computational time to determine the first open channel is much lower (seconds to minutes) than that required to solve the full fluid flow problem using optimization methods (days to weeks) (Dimakopoulos *et al.* 2018; Chaparian & Tammisola 2021).

3. Results

3.1. *The first open channel*

When the applied pressure drop approaches the critical value $\Delta P \to \Delta P_c^+$, there exists a single open channel across the entire medium. Here, we test the validity of the proposed approach to determine the first open channel when the solid–liquid transition occurs. For comparison, we solve the full flow field under pressure-driven conditions for a yield-stress fluid for the porous media shown in figure 2. We consider the cases of $\phi = 0.3$ and $\phi = 0.5$, respectively. All the lengths are normalized with the macroscopic length of the system L and also $R_s/L = 0.02$ and $R_s/L = 0.1$. In this study, we investigate two-dimensional porous media, however, the network approach is general and can also be used to study three-dimensional geometries.

Figure 2(*a*) shows the normalized velocity magnitude from the solution of the momentum equation (i.e. Stokes equation) for a Bingham fluid (Chaparian & Tammisola 2021). Details of the numerical simulation of the fluid flow problem shown in figure 2(*a*) are discussed by Chaparian & Tammisola (2021). To highlight, the porous medium is designed with a desirable porosity by randomizing non-overlapping monodisperse discs. To solve the equations of motion (Stokes equation), we use the augmented Lagrangian method implemented in a finite element environment (FreeFEM++; see Hecht 2012) coupled with adaptive mesh (Roquet & Saramito 2003). At the inlet (left side of

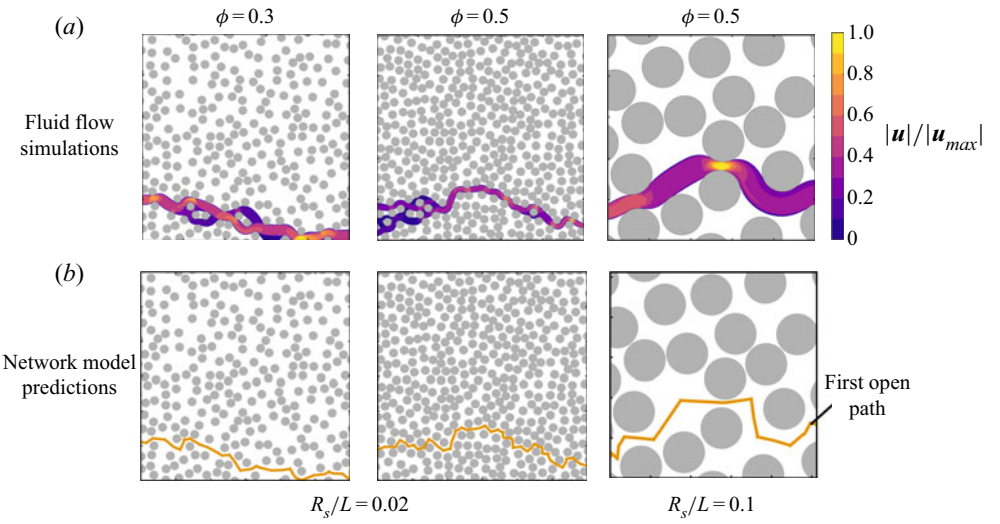

Figure 2. Validation of the network model for the first open channel against simulations for a pressure-driven Bingham fluid in a porous medium with $R_s/L = 0.02$ and $R_s/L = 0.1$. (*a*) Simulation results of the open pathway for conditions near the critical pressure drop ΔP_c. The contour plot shows the magnitude of the local velocity, normalized with the maximum velocity across the channel. (*b*) Network model predictions for the first open channel. The cases of $\phi = 0.3$ and $\phi = 0.5$ are examined. It is clear that both the full Bingham fluid simulation and the network model predict the same location for the first open channel.

the computational box) we set the flow rate (see Roustaei & Frigaard (2015), for the algorithm), and as a result, we calculate the pressure drop for different values of yield stress. More precisely, the velocity is scaled with the average inlet velocity U, hence, the non-dimensional flow rate is always equal to unity. Therefore, the yield limit is transferred to $\tau_y \ell_{ch}/\mu U \to \infty$ (i.e. Bingham number $\to \infty$), where ℓ_{ch} is a characteristic length. When $\tau_y \ell_{ch}/\mu U \to \infty$ the non-dimensional pressure drop goes to infinity as well $\Delta P \ell_{ch}^2/\mu U L \to \infty$. However, the ratio of the non-dimensional pressure drop to the Bingham number, $\Delta P \ell_{ch}/\tau_y L$ or the yield number, is of interest, which at this limit asymptotically reaches a finite value. So the limiting pressure drop to open the first channel can be computed by considering the limit $\tau_y \ell_{ch}/\mu U \to \infty$. For more details, we refer the interested reader to Chaparian *et al.* (2020) and Chaparian & Tammisola (2021).

Figure 2(*b*) depicts the predictions for the first open channel after solving the minimization problem of (2.2). In all cases (i.e. $\phi = 0.3$ and 0.5 and $R_s/L = 0.02$ and 0.1), the network model is able to reproduce the results of the fluid flow problem (i.e. (*a*)) for the first open path. In the full fluid flow problem for $R_s/L = 0.02$, we can see the existence of minor tiny 'roundabout' paths in the vicinity of the major path. However, it is clear from figure 2(*a*) that the flow rate in those minor paths is negligible and does not contribute to the leading order of the dissipation that is attributed to the major route predicted by the network model, figure 2(*b*).

3.2. *Critical pressure drop ΔP_c and its statistics in porous media*

In addition to the first open path, the network model can predict the critical pressure difference ΔP_c required to yield the fluid in the porous medium.

In table 1 we show the predictions of the normalized critical pressure drop $\Delta P_c/\tau_y$ for both the network model and the full simulations. For $\phi = 0.3$ and 0.5 we consider the

ϕ	R_s/L	$\frac{\Delta P_c}{\tau_y}$ network	$\frac{\Delta P_c}{\tau_y}$ simulations	Rel. error %
0.1	0.02	22.16	22.63	1.87
0.3	0.02	61	65.2	6.43
0.5	0.02	142.16	145.28	2.05
0.5	0.1	36.7817	32.7868	12.18

Table 1. Predicted normalized critical pressure drop ΔP_c required to open the first open channel for the configurations shown in figure 2. We show both the predictions of the network model and the full simulation results, along with the relative error $(\Delta P_c^{sim} - \Delta P_c^{net})/\Delta P_c^{sim}$. The network model is adequate on predicting both the first open channel and the critical pressure drop required to open it.

configurations shown in figure 2. In the cases of $R_s/L = 0.02$, it is clear that the relative difference in the predicted ΔP_c by the two approaches never exceeds 6.5 %. The negligible difference can be justified by the simplification of the geometric characteristics of the medium by its network representation. For $R_s/L = 0.1$, the relative error is approximately 12.1 %, which we attribute to the large curvature effects of the discs that the network model cannot capture. We conclude, however, that network-based models are adequate to predict both the first open path and the critical pressure drop required to open it.

Before we proceed with the analysis of the model, we want to comment on the choice of h_i and ℓ_i for calculating the critical pressure drop. Given the geometric irregularities of porous media, the choice of the local geometric quantities present in the model is non-trivial. Here, in the case of non-overlapping discs, we used the h_i and ℓ_i that were directly calculated by the maximum-ball algorithm. Other choices are possible, where for instance one can use the equivalent gap length for evaluating h_i defined as the ratio of the area of the channel to its perimeter. To better understand the influence of such a choice, we repeated the calculations for $\phi = 0.5$ and $R_s/L = 0.02$ where now h_i is the equivalent gap length and has been extracted by the image processing methods described by Gostick *et al.* (2019). While the results for the first open path are identical, we find $\Delta P_{c,equiv}/\tau_y \simeq 1016.6$, which is an order of magnitude larger than the fluid flow simulation predictions. This comparison indicates that the critical pressure drop is sensitive to the choice of h_i and ℓ_i, however, the location as well as the topology of the first open path tend to be unchanged.

The validation of the model allows us to predict ΔP_c as a function of ϕ and the geometric characteristics of the system. For a porous medium made of non-overlapping monodispersed discs, we control the microstructure characteristics by changing the ratio R_s/L. For each combination of ϕ and R_s/L, we generate 500 realizations to gather the statistics of ΔP_c.

Figure 3(*a*) shows the normalized critical pressure drop $\Delta P_c/\tau_y$ in terms of ϕ. The coloured lines indicate different values of $R_s/L \in [0.02, 0.1]$, while the error bars correspond to the variance of the statistical sample. For all R_s/L the normalized pressure drop increases with increasing ϕ. This behaviour is expected as h_i of each edge decreases monotonically as ϕ increases (Torquato & Haslach 2002). Additionally, we observe that decreasing the ratio R_s/L leads to an increase in ΔP_c, in qualitative agreement with experiments (Waisbord *et al.* 2019). The reason for this behaviour can be explained by examining the arclength (defined as $L_c = \sum_i^N \ell_i$) for the first open channel.

Figure 3(*b*) illustrates the histogram of L_c for $\phi = 0.3$ and 0.5 as well as $R_s/L = 0.02$ and 0.08. In both cases we observe that increasing the solid volume fraction leads to an

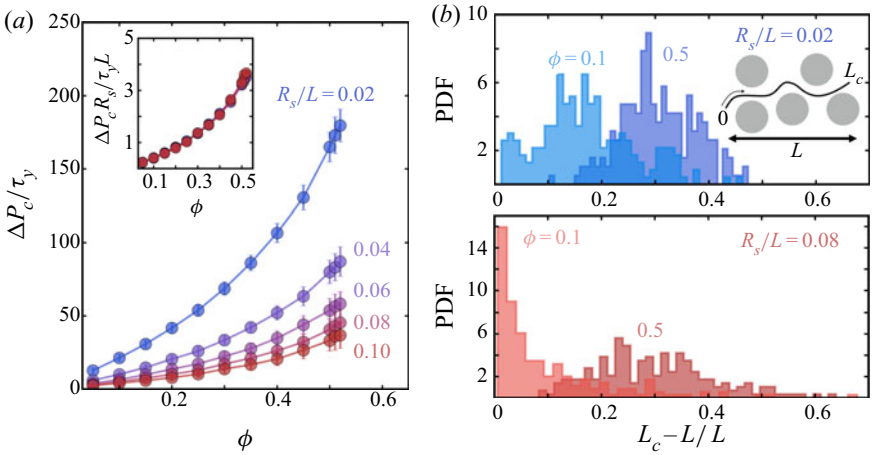

Figure 3. Statistics of the predictions of the network model for 500 realizations per value of ϕ. (*a*) Critical pressure drop ΔP_c as a function of the volume fraction ϕ for different ratios of R_s/L; ΔP_c is normalized with the yield stress of the fluid τ_y. The error bars indicate the variance around the mean value. Inset – scaled critical pressure drop $\Delta P_c R_s/\tau_y L$ in terms of ϕ. For non-overlapping discs, the results for different R_s/L collapse into a master curve. (*b*) Probability density distributions for the normalized arclength of the first open channel $L_c/L - 1$. The cases of $R_s/L = 0.02$ and $R_s/L = 0.08$ are shown, respectively, for $\phi = 0.1$ and $\phi = 0.5$. In general, increasing ϕ leads to increase of ΔP_c required to open the first channel, but also leads to a wide distribution of arclengths, which provide a large uncertainty in the critical macroscopic pressure gradient $\Delta P_c/L_c$ required to yield the fluid in the porous medium.

increase in the total length of the first open path. While large ϕ results in almost similar behaviour for both R_s/L, it is apparent that decreasing the size of the discs results in more tortuous paths, even for low solid volume fraction.

Dimensional analysis of (2.2) indicates that ΔP_c follows a simple scaling with R_s/L. In particular, by rescaling the local h_i with the discs radius R_s, we find $\Delta\tilde{P}_c = \Delta P_c R_s/\tau_y L = \sum_{i=1}^{N} (\ell_i/L)(R_s/h_i)$. This form can be interpreted as the ratio between the applied pressure drop $\Delta P/L$ over the local shear force per volume generated by the existence of particles with radius R_s.

The inset in figure 3(*a*) shows the rescaled form of the critical pressure drop for all R_s/L, where for non-overlapping discs a mastercurve exists for all the examined values of ϕ. To better understand the functional dependence of $\Delta\tilde{P}_c$ with ϕ, we follow a mean-field approach and approximate its expression as

$$\Delta\tilde{P}_c \simeq N\left\langle\frac{\ell}{L}\right\rangle\left\langle\frac{R_s}{h}\right\rangle = \left\langle\frac{L_c}{L}\right\rangle\left\langle\frac{R_s}{h}\right\rangle, \tag{3.1}$$

where N is the number of segments of the path, while $\langle\ell\rangle$ and $\langle 1/h\rangle$ are the mean length and inverse gap of each edge, respectively. To find the functional dependence for both $\langle L_c/L\rangle$ and $\langle R_s/h\rangle$, we calculate their average directly from our collected data values where we find $\langle L_c/L\rangle \sim 0.5\phi$ and $\langle R_s/h\rangle \sim 2/(1-\phi)$; see figures 4(*a*) and 4(*b*). In the porous medium community, L_c/L is known as the geometric tortuosity τ_g and several analytical and empirical relations have been proposed to describe its form as a function of the porosity $(1-\phi)$ (Guo 2012). To a first approximation, we describe $\langle L_c/L\rangle$ with the Bruggeman relation for cylinders $\langle L_c/L\rangle \sim (1-\phi)^{-1/2}$ (Tjaden *et al.* 2016). In the limit of $\phi \to 0$, we find $\langle L_c/L\rangle \simeq 1 + 0.5\phi + O(\phi^2)$, which shows a very similar behaviour to the scaling reported in figure 4(*b*). While this limit corresponds to a dilute mixture of particles

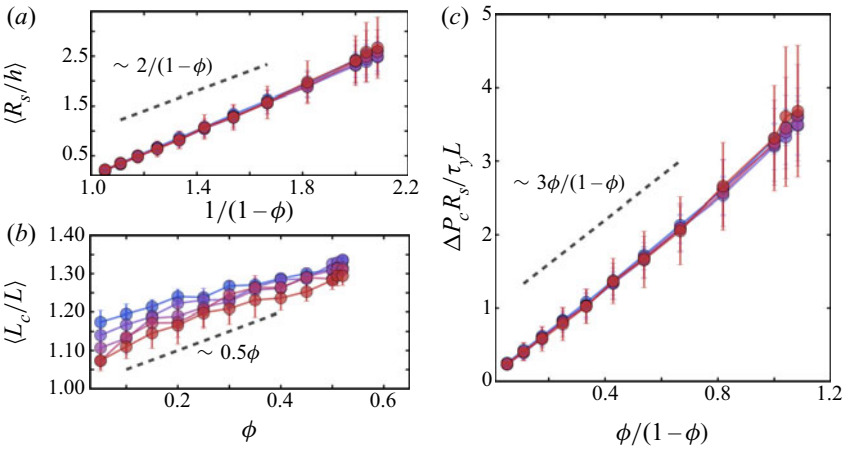

Figure 4. Scalings of the geometric characteristics of a porous medium made of non-overlapping discs. (*a*) Inverse channel gap $\langle R_s/h \rangle$ thickness vs. $(1-\phi)^{-1}$. From our calculations it is clear that $\langle R_s/h \rangle$ scales with the inverse of the porosity $1-\phi$. (*b*) First open channel length $\langle L_c/L \rangle$ vs. ϕ. Based on a simple estimate of the geometric tortuosity, we find that $\langle L_c/L \rangle$ scales linearly with ϕ. (*c*) Non-dimensional pressure gradient $\Delta\tilde{P}_c = \Delta P_c R_s/\tau_y L$ vs. $\phi/(1-\phi)$. According to (3.1), the product of $\langle L_c/L \rangle$ and $\langle R_s/h \rangle$ indicates that $\Delta\tilde{P}_c$ scales with $\phi/(1-\phi)$.

in a permeable matrix, the geometric characteristics of the first open roughly follow this estimation in the range of studied porosities.

To this end, we can approximate $\Delta\tilde{P}_c \simeq Af(\phi)$ for monodisperse discs of radius R_s, where A is a proportionality constant and $f(\phi) = \phi/(1-\phi)$. In figure 4(*c*) we show the dimensionless pressure drop $\Delta\tilde{P}_c$ vs. $f(\phi)$, where we see a linear relationship between the two quantities, with $A \simeq 3$, validating the mean-field assumption considered in (3.1).

4. Summary and discussion

4.1. *Summary*

In this work, we investigated the application of network models for yield-stress fluids in porous media. We find that network models provide an efficient and accurate way to describe the fluidization conditions in porous media. In particular, they capture the first open channel, which is equivalent to the path of least resistance through the entire medium. We also demonstrated the capabilities of the network model to predict the critical applied pressure drop required to open the first channel in the medium. This was rationalized by comparing the network results with direct numerical simulations of the fluid flow problem. We showed the accuracy and computational efficiency of the network-based models in the context of solid–liquid transition. Also, we performed statistical analyses on different two-dimensional porous media made of non-overlapping discs to understand the dependence of the critical pressure drop ΔP_c on the solid volume fraction ϕ and the geometric characteristics of the solid matrix. For two-dimensional porous media that consist of non-overlapping discs, we revealed that the ratio $\Delta P_c R_s/\tau_y L$ scales linearly with $\phi/(1-\phi)$, which is a result of the average geometric characteristics of the first open path.

4.2. *Discussion*

The present model considers only the case of viscoplastic materials and disregards the fluid elasticity (Saramito 2007; Fraggedakis, Dimakopoulos & Tsamopoulos 2016*a*,*b*;

Chaparian *et al.* 2020) prior to yielding. Therefore, further analysis is required to connect the yield criterion to the elastic modulus of the fluid, which can provide insights for engineering both the porous medium and the fluid itself. Additionally, the yielding and/or stoppage conditions might be further affected by possible thixotropic (Mewis & Wagner 2012) and kinematic hardening (Gurtin *et al.* 2010; Dimitriou & McKinley 2019) phenomena.

Beyond the rheological characteristics of the model, more complete closures for the yielding criterion, (2.2), can be considered that take into account the geometric irregularities of the channels. For instance, Roustaei *et al.* (2016) showed that $\Delta P_{c,i}$, even for quite smooth channels, can be up to 25 % different compared to that predicted for a typical planar Poiseuille flow. Also, irregular channels that show fracture-like characteristics tend to yield at a smaller applied pressure drop compared to straight channels. Another complication on the yield-stress criterion might come from the dimensionality of the porous medium. In three-dimensional structures, the description of open channels as tubes might not be adequate, and the geometric quantities h_i and ℓ_i need to be chosen carefully (Waisbord *et al.* 2019). Thus, for irregular porous media, the yielding criterion, and thus the expression related to the minimum pressure to open the first channel, should be modified.

The mean-field approximation for the critical pressure drop $\Delta\tilde{P}_c$ as given in (3.1), indicates that one can develop analytical approximations for the critical pressure drop based only on geometries quantities of a medium that consists of non-overlapping objects. In particular, one can follow a more rigorous approach to estimate $\langle R_s/h\rangle$ analytically, as presented by Torquato & Haslach (2002). In particular, $\langle R_s/h\rangle = \langle 1/(l-1)\rangle$ where l is the nearest-neighbour distance between particles, and can be formally calculated as

$$\left\langle \frac{1}{l-1} \right\rangle = \int_1^\infty \frac{1}{l-1} H_P(l)\,\mathrm{d}l, \tag{4.1}$$

where H_P is the 'particle' nearest-neighbour probability density function and depends on the geometry and dimensionality of the particles (Torquato, Lu & Rubinstein 1990) as well as on the protocol used to generate the particle configuration. The random sequential addition algorithm used here produces non-equilibrium configurations where no analytical expressions for H_P are known. However, when equilibrium configurations are generated (e.g. through Monte Carlo algorithms), Torquato (1995) has reported exact and approximate expressions for H_P for monodisperse rods, discs and spheres.

Our results on the normalized critical pressure drop can be used to design porous media systems with the desired flow properties. In applications such as semi-solid flow batteries (Duduta *et al.* 2011), it is critical to keep the contact between the active material (electrode particles) and the conductive wiring (carbon nanoparticle network) intact during operation (Wei *et al.* 2015). This can be achieved by immersing the active material and the electronically conductive agent in yield-stress fluids like Carbopol (Zhu *et al.* 2020). Therefore, we can use the predicted $\Delta P_c/\tau_y$ to determine the size of the active particles to optimize the design and operation of semi-solid electrodes.

The present model can also provide insights into the design of porous media. By taking advantage of the computational efficiency of the proposed network model, we can perform on-the-fly optimization to construct porous media with optimal mixing and transport properties (Lester, Metcalfe & Trefry 2013). Such ideas have recently been implemented in elastic networks with optimal phonon band structures (Ronellenfitsch & Dunkel 2019), and we believe they can also be used for designing porous media immersed in yield-stress fluids.

Given their inherent node/edge structure, network models are fairly simple to analyse using graph theoretical tools. The unique property of yield-stress fluid, namely the fluidization condition, allows us to use algorithms that can find the minimum resistance pathways with minimal effort. In coarse-grained domains, however, where the microscopic geometric irregularities are encoded in the heterogeneous 'permeability' tensor (Hewitt *et al.* 2016), graph theory tools might not be the most suitable ones. An alternative way to calculate the first open channel in a continuum with spatially variable properties is through methodologies used in physical chemistry to identify reaction pathways (Henkelman, Uberuaga & Jónsson 2000). There, the first open channel corresponds to the path that passes through the minimum energy barrier, namely the transition state point.

Acknowledgements. D.F. (aka dfrag) wants to thank T. Zhou, M. Mirzadeh, A. Sahu and Y. Dimakopoulos for insightful discussions related to the validity of the network model.

Declaration of interest. The authors report no conflict of interest.

Author ORCIDs.
Dimitrios Fraggedakis https://orcid.org/0000-0003-3301-6255;
Emad Chaparian https://orcid.org/0000-0002-5397-2079;
Outi Tammisola https://orcid.org/0000-0003-4317-1726.

Author contributions. D.F. conceptualized and designed the present study. D.F. and E.C. performed the analysis and contributed equally in the present work. D.F. wrote the first version of the present manuscript. All authors contributed to the final manuscript.

References

Al-Kharusi, A.S. & Blunt, M.J. 2007 Network extraction from sandstone and carbonate pore space images. *J. Petrol. Sci. Engng* **56** (4), 219–231.

Alim, K., Parsa, S., Weitz, D.A. & Brenner, M.P. 2017 Local pore size correlations determine flow distributions in porous media. *Phys. Rev. Lett.* **119** (14), 144501.

Aufrecht, J.A., Fowlkes, J.D., Bible, A.N., Morrell-Falvey, J., Doktycz, M.J. & Retterer, S.T. 2019 Pore-scale hydrodynamics influence the spatial evolution of bacterial biofilms in a microfluidic porous network. *PLoS ONE* **14** (6), e0218316.

Balhoff, M. 2005 Modeling the flow of non-Newtonian fluids in packed beds at the pore scale. PhD thesis, Louisiana State University.

Balhoff, M., Sanchez-Rivera, D., Kwok, A., Mehmani, Y. & Prodanović, M. 2012 Numerical algorithms for network modeling of yield stress and other non-Newtonian fluids in porous media. *Transp. Porous Med.* **93** (3), 363–379.

Balhoff, M.T. & Thompson, K.E. 2004 Modeling the steady flow of yield-stress fluids in packed beds. *AIChE J.* **50** (12), 3034–3048.

Balmforth, N.J., Frigaard, I.A. & Ovarlez, G. 2014 Yielding to stress: recent developments in viscoplastic fluid mechanics. *Annu. Rev. Fluid Mech.* **46**, 121–146.

Barenblatt, G.I., Entov, V.M. & Ryzhik, V.M. 1989 *Theory of Fluid Flows through Natural Rocks*. Kluwer Academic Publishers.

Bauer, D., Talon, L., Peysson, Y., Ly, H.B., Batôt, G., Chevalier, T. & Fleury, M. 2019 Experimental and numerical determination of Darcy's law for yield stress fluids in porous media. *Phys. Rev. Fluids* **4** (6), 063301.

Blunt, M.J. 2001 Flow in porous media—pore-network models and multiphase flow. *Curr. Opin. Colloid Interface Sci.* **6** (3), 197–207.

Blunt, M.J., Bijeljic, B., Dong, H., Gharbi, O., Iglauer, S., Mostaghimi, P., Paluszny, A. & Pentland, C. 2013 Pore-scale imaging and modelling. *Adv. Water Resour.* **51**, 197–216.

Bollobás, B. 2013 *Modern Graph Theory*, vol. 184. Springer Science & Business Media.

Bonn, D. & Denn, M.M. 2009 Yield stress fluids slowly yield to analysis. *Science* **324** (5933), 1401–1402.

Bryant, S.L., King, P.R. & Mellor, D.W. 1993 Network model evaluation of permeability and spatial correlation in a real random sphere packing. *Transp. Porous Med.* **11** (1), 53–70.

Chaparian, E., Izbassarov, D., De Vita, F., Brandt, L. & Tammisola, O. 2020 Yield-stress fluids in porous media: a comparison of viscoplastic and elastoviscoplastic flows. *Meccanica* **55** (2), 331–342.

Chaparian, E. & Tammisola, O. 2021 Sliding flows of yield-stress fluids. Accepted for publication in *J. Fluid Mech.* (preprint) arXiv:2004.02950.

Chen, M., Rossen, W. & Yortsos, Y.C. 2005 The flow and displacement in porous media of fluids with yield stress. *Chem. Engng Sci.* **60** (15), 4183–4202.

Cule, D. & Torquato, S. 1999 Generating random media from limited microstructural information via stochastic optimization. *J. Appl. Phys.* **86** (6), 3428–3437.

De Groot, S.R. & Mazur, P. 1984 *Non-Equilibrium Thermodynamics*. Dover Publication Inc.

Dijkstra, E.W. 1959 A note on two problems in connexion with graphs. *Numer. Math.* **1** (1), 269–271.

Dimakopoulos, Y., Makrigiorgos, G., Georgiou, G.C. & Tsamopoulos, J. 2018 The PAL (Penalized Augmented Lagrangian) method for computing viscoplastic flows: a new fast converging scheme. *J. Non-Newtonian Fluid Mech.* **256**, 23–41.

Dimakopoulos, Y., Pavlidis, M. & Tsamopoulos, J. 2013 Steady bubble rise in Herschel–Bulkley fluids and comparison of predictions via the augmented Lagrangian method with those via the Papanastasiou model. *J. Non-Newtonian Fluid Mech.* **200**, 34–51.

Dimitriou, C.J. & McKinley, G.H. 2019 A canonical framework for modeling elasto-viscoplasticity in complex fluids. *J. Non-Newtonian Fluid Mech.* **265**, 116–132.

Dong, H. & Blunt, M.J. 2009 Pore-network extraction from micro-computerized-tomography images. *Phys. Rev.* E **80** (3), 036307.

Duduta, M., Ho, B., Wood, V.C., Limthongkul, P., Brunini, V.E., Carter, W.C. & Chiang, Y. 2011 Semi-solid lithium rechargeable flow battery. *Adv. Energy Mater.* **1** (4), 511–516.

Entov, V.M. 1967 On some two-dimensional problems of the theory of filtration with a limiting gradient. *Prikl. Mat. Mekh.* **31** (5), 820–833.

Farajzadeh, R., Andrianov, A., Krastev, R., Hirasaki, G.J. & Rossen, W.R. 2012 Foam–oil interaction in porous media: implications for foam assisted enhanced oil recovery. *Adv. Colloid Interface Sci.* **183**, 1–13.

Fatt, I. 1956 The network model of porous media. *Trans. AIME* **207** (1), 144–181.

Fraggedakis, D., Dimakopoulos, Y. & Tsamopoulos, J. 2016*a* Yielding the yield-stress analysis: a study focused on the effects of elasticity on the settling of a single spherical particle in simple yield-stress fluids. *Soft Matt.* **12** (24), 5378–5401.

Fraggedakis, D., Dimakopoulos, Y. & Tsamopoulos, J. 2016*b* Yielding the yield stress analysis: a thorough comparison of recently proposed elasto-visco-plastic (EVP) fluid models. *J. Non-Newtonian Fluid Mech.* **236**, 104–122.

Fraggedakis, D., Kouris, C., Dimakopoulos, Y. & Tsamopoulos, J. 2015 Flow of two immiscible fluids in a periodically constricted tube: transitions to stratified, segmented, churn, spray, or segregated flow. *Phys. Fluids* **27** (8), 082102.

Frigaard, I.A. 2019 Background lectures on ideal visco-plastic fluid flows. In *Lectures on Visco-Plastic Fluid Mechanics*, pp. 1–40. Springer.

Frigaard, I.A. & Nouar, C. 2005 On the usage of viscosity regularisation methods for visco-plastic fluid flow computation. *J. Non-Newtonian Fluid Mech.* **127** (1), 1–26.

Frigaard, I.A., Paso, K.G. & de Souza Mendes, P.R. 2017 Bingham's model in the oil and gas industry. *Rheol. Acta* **56** (3), 259–282.

Glowinski, R. 2008 *Lectures on Numerical Methods for Non-Linear Variational Problems*. Springer Science & Business Media.

Glowinski, R. & Wachs, A. 2011 On the numerical simulation of viscoplastic fluid flow. In *Handbook of Numerical Analysis*, vol. 16, pp. 483–717. Elsevier.

Gostick, J.T. 2017 Versatile and efficient pore network extraction method using marker-based watershed segmentation. *Phys. Rev.* E **96** (2), 023307.

Gostick, J.T., Khan, Z.A., Tranter, T.G., Kok, M.D.R., Agnaou, M., Sadeghi, M. & Jervis, R. 2019 Porespy: a python toolkit for quantitative analysis of porous media images. *J. Open Source Softw.* **4** (37), 1296.

Green, D.W. & Willhite, G.P. 1998 *Enhanced Oil Recovery*, vol. 6. Society of Petroleum Engineers.

Greenkorn, R.A. 1983 *Flow Phenomena in Porous Media: Fundamentals and Applications in Petroleum, Water and Food Production*. Marcel Dekker.

Guo, P. 2012 Dependency of tortuosity and permeability of porous media on directional distribution of pore voids. *Transp. Porous Med.* **95** (2), 285–303.

Gurtin, M.E., Fried, E. & Anand, L. 2010 *The Mechanics and Thermodynamics of Continua*. Cambridge University Press.

HAGBERG, A., SWART, P. & CHULT, D.S. 2008 Exploring network structure, dynamics, and function using NetworkX. *Tech. Rep.* Los Alamos National Laboratory (LANL).

HECHT, F. 2012 New development in freefem++. *J. Numer. Math.* **20** (3), 251–265.

HENKELMAN, G., UBERUAGA, B.P. & JÓNSSON, H. 2000 A climbing image nudged elastic band method for finding saddle points and minimum energy paths. *J. Chem. Phys.* **113** (22), 9901–9904.

HERZIG, J.P., LECLERC, D.M. & GOFF, P.L. 1970 Flow of suspensions through porous media–application to deep filtration. *Ind. Engng Chem. Res.* **62** (5), 8–35.

HESTENES, M.R. 1969 Multiplier and gradient methods. *J. Optim. Theor. Applics.* **4** (5), 303–320.

HEWITT, D.R., DANESHI, M., BALMFORTH, N.J. & MARTINEZ, D.M. 2016 Obstructed and channelized viscoplastic flow in a Hele-Shaw cell. *J. Fluid Mech.* **790**, 173–204.

HILL, R. 1998 *The Mathematical Theory of Plasticity*, vol. 11. Oxford University Press.

HUILGOL, R.R. 2015 *Fluid Mechanics of Viscoplasticity*. Springer.

JAISI, D.P., SALEH, N.B., BLAKE, R.E. & ELIMELECH, M. 2008 Transport of single-walled carbon nanotubes in porous media: filtration mechanisms and reversibility. *Environ. Sci. Technol.* **42** (22), 8317–8323.

KHARABAF, H. & YORTSOS, Y.C. 1997 Invasion percolation with memory. *Phys. Rev.* E **55** (6), 7177.

LESTER, D.R., METCALFE, G. & TREFRY, M.G. 2013 Is chaotic advection inherent to porous media flow? *Phys. Rev. Lett.* **111** (17), 174101.

LIU, C., DE LUCA, A., ROSSO, A. & TALON, L. 2019 Darcy's law for yield stress fluids. *Phys. Rev. Lett.* **122** (24), 245502.

MEWIS, J. & WAGNER, N.J. 2012 *Colloidal Suspension Rheology*. Cambridge University Press.

PANDEY, A. 2003 Solid-state fermentation. *Biochem. Engng J.* **13** (2–3), 81–84.

PAPANASTASIOU, T.C. 1987 Flows of materials with yield. *J. Rheol.* **31** (5), 385–404.

POWELL, M.J.D. 1978 Algorithms for nonlinear constraints that use Lagrangian functions. *Math. Program.* **14** (1), 224–248.

RONELLENFITSCH, H. & DUNKEL, J. 2019 Chiral topological phases in designed mechanical networks. *Front. Phys.* **7**, 178.

ROQUET, N. & SARAMITO, P. 2003 An adaptive finite element method for Bingham fluid flows around a cylinder. *Comput. Meth. Appl. Mech. Engng* **192** (31), 3317–3341.

ROUSTAEI, A., CHEVALIER, T., TALON, L. & FRIGAARD, I.A. 2016 Non-darcy effects in fracture flows of a yield stress fluid. *J. Fluid Mech.* **805**, 222–261.

ROUSTAEI, A. & FRIGAARD, I.A. 2015 Residual drilling mud during conditioning of uneven boreholes in primary cementing. Part 2: steady laminar inertial flows. *J. Non-Newtonian Fluid Mech.* **226**, 1–15.

SAHIMI, M. 2011 *Flow and Transport in Porous Media and Fractured Rock: From Classical Methods to Modern Approaches*. John Wiley & Sons.

SARAMITO, P. 2007 A new constitutive equation for elastoviscoplastic fluid flows. *J. Non-Newtonian Fluid Mech.* **145** (1), 1–14.

SARAMITO, P. 2016 *Complex Fluids*. Springer.

SARAMITO, P. & WACHS, A. 2017 Progress in numerical simulation of yield stress fluid flows. *Rheol. Acta* **56** (3), 211–230.

SCHLESINGER, W.H. 1999 Carbon sequestration in soils. *Science* **284** (5423), 2095.

SILIN, D. & PATZEK, T. 2006 Pore space morphology analysis using maximal inscribed spheres. *Phys.* A **371** (2), 336–360.

SOCHI, T. 2005 Pore-scale modeling of non-Newtonian flow in porous media. PhD thesis, Imperial College London.

STOOP, N., WAISBORD, N., KANTSLER, V., HEINONEN, V., GUASTO, J.S. & DUNKEL, J. 2019 Disorder-induced topological transition in porous media flow networks. *J. Non-Newtonian Fluid Mech.* **268**, 66–74.

SUN, H., ZHU, J., BAUMANN, D., PENG, L., XU, Y., SHAKIR, I., HUANG, Y. & DUAN, X. 2019 Hierarchical 3D electrodes for electrochemical energy storage. *Nat. Rev. Mater.* **4** (1), 45–60.

TALON, L., AURADOU, H., PESSEL, M. & HANSEN, A. 2013 Geometry of optimal path hierarchies. *Europhys. Lett.* **103** (3), 30003.

TALON, L. & HANSEN, A. 2020 Effective rheology of bi-viscous non-Newtonian fluids in porous media. *Front. Phys.* **7**, 225.

TIEN, C. & PAYATAKES, A.C. 1979 Advances in deep bed filtration. *AIChE J.* **25** (5), 737–759.

TJADEN, B., COOPER, S.J., BRETT, D.J.L., KRAMER, D. & SHEARING, P.R. 2016 On the origin and application of the bruggeman correlation for analysing transport phenomena in electrochemical systems. *Curr. Opin. Chem. Engng* **12**, 44–51.

TORQUATO, S. 1995 Nearest-neighbor statistics for packings of hard spheres and disks. *Phys. Rev.* E **51** (4), 3170.

TORQUATO, S. & HASLACH, H.W. JR. 2002 Random heterogeneous materials: microstructure and macroscopic properties. *Appl. Mech. Rev.* **55** (4), B62–B63.

TORQUATO, S., LU, B. & RUBINSTEIN, J. 1990 Nearest-neighbor distribution functions in many-body systems. *Phys. Rev.* A **41** (4), 2059.

TORQUATO, S., UCHE, O.U. & STILLINGER, F.H. 2006 Random sequential addition of hard spheres in high Euclidean dimensions. *Phys. Rev.* E **74** (6), 061308.

TSAMOPOULOS, J., DIMAKOPOULOS, Y., CHATZIDAI, N., KARAPETSAS, G. & PAVLIDIS, M. 2008 Steady bubble rise and deformation in Newtonian and viscoplastic fluids and conditions for bubble entrapment. *J. Fluid Mech.* **601**, 123–164.

WAISBORD, N., STOOP, N., WALKAMA, D.M., DUNKEL, J. & GUASTO, J.S. 2019 Anomalous percolation flow transition of yield stress fluids in porous media. *Phys. Rev. Fluids* **4** (6), 063303.

WEI, T., FAN, F.Y., HELAL, A., SMITH, K.C., MCKINLEY, G.H., CHIANG, Y. & LEWIS, J.A. 2015 Biphasic electrode suspensions for li-ion semi-solid flow cells with high energy density, fast charge transport, and low-dissipation flow. *Adv. Energy Mater.* **5** (15), 1500535.

ZHANG, G. & TORQUATO, S. 2013 Precise algorithm to generate random sequential addition of hard hyperspheres at saturation. *Phys. Rev.* E **88** (5), 053312.

ZHU, Y., *et al.* 2020 High-energy and high-power Zn-Ni flow batteries with semi-solid electrodes. *Sustain. Energy Fuels* **4**, 4076.